IEEE Access
Multidisciplinary ⋮ Rapid Review ⋮ Open Access Journal

Received 6 September 2023, accepted 24 September 2023, date of publication 29 September 2023,
date of current version 9 October 2023.

Digital Object Identifier 10.1109/ACCESS.2023.3320802

RESEARCH ARTICLE

An Electrically Reconfigurable Circularly-Polarized Planar Array Antenna With Built-In Bias-Isolation Mechanism

HTET WAI HTUN, (Graduate Student Member, IEEE), EISUKE NISHIYAMA, (Member, IEEE), AND ICHIHIKO TOYODA, (Member, IEEE)
Graduate School of Science and Engineering, Saga University, Saga 840-8502, Japan
Corresponding author: Htet Wai Htun (htun@ceng.ec.saga-u.ac.jp)

ABSTRACT This paper proposes a novel design of a reconfigurable microstrip array antenna for circular polarization (CP) switching function. The proposed array is implemented in a 2×2 arrangement using four patch elements and a feed network. The bias-isolation mechanism is an integral feature of this array design, and it is facilitated by the short-ended microstrip lines and planar magic-Ts. By this approach, both the radiating elements and feed structure ensure the straightforward RF-DC isolation method with no auxiliary passive components and filters. Also, with the superb integration of these two techniques, the entire array is viable in a single-layer configuration, featuring design freedom for a larger array. Furthermore, the CP switching function can simply be achieved by controlling the bias state of the diodes. To verify the proposed concept, prototype antennas are fabricated and tested. The measured results demonstrate that the proposed array can function as a CP reconfigurable antenna with simple bias-isolation method.

INDEX TERMS Bias isolation, circular polarization, electrical reconfiguration, magic-T, planar antenna, short-ended microstrip lines.

I. INTRODUCTION

Planar integrated antenna technology has consistently made significant contributions to the advancement of wireless communication systems. With this technology, the antenna configurations can be made to be compact, simple, cost-effective, and easily manufactured. Also, its adaptable characteristics offers an easy integration with the various techniques for a wide range of applications. Therefore, many single-element and array designs of planar integrated antennas have been developed to date for the intended functions.

Many excellent studies have shown that the polarization reconfiguration is one of the well-known functionalities that can be combined with the planar integrated antennas. It is noted that this function can be actualized using mechanical [1], electrical [2], optical [3] and material controls [4]. Among them, the electrical reconfiguration method has tremendously matured alongside with the planar antennas. Using the switching and tunable components (PIN diodes, MEMS, and varactors etc.), the antenna's operation can electrically be activated for the desired polarization modes. For this reason, many single-element designs are increasingly prevalent in the field of polarization switching study. In literatures, numerous designs have introduced the perturbation technique as a means of CP reconfiguration. For this functionality, the authors reported the several patch antenna designs with integrated bias-circuit perturbations [5], [6], [7], [8]. Alternatively, the slot formation [9], [10], [11] can be authenticated as another CP reconfigurable strategy. This method uses the switchable slots in the antenna structures to alter the current distribution behavior for CP excitation. Moreover, the polarization reconfigurable antennas can be designed using the switchable feed networks [12], [13], [14], [15], [16], [17], [18]. In this approach, the desired change in various polarization modes can be achieved by adjusting the necessary phase shift of the feed lines. Furthermore,

The associate editor coordinating the review of this manuscript and approving it for publication was Tutku Karacolak.

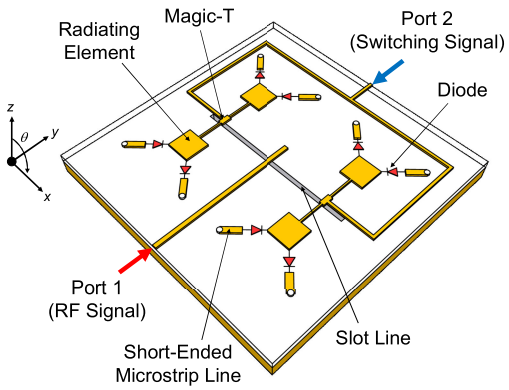

FIGURE 1. Structure of the proposed 2 × 2 CP reconfigurable microstrip array antenna.

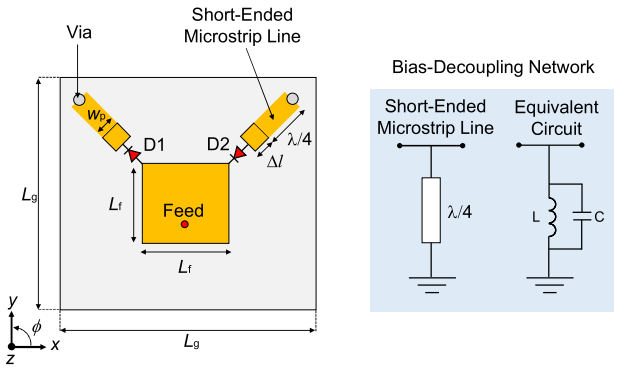

FIGURE 2. Structure of the CP reconfigurable element and its equivalent bias-decoupling network.

the authors described that double-balanced multiplier (DBM) loaded antennas [19], [20], [21], [22] are able to operate for CP switching performance. Recently, the use of reconfigurable stacked configurations has significantly improved the antenna performances in terms of wideband characteristics [23], [24], [25], [26], high gain [27] and high efficiency [28]. Also, a profusion of research is getting concentrated on array architectures, which can enable the polarization reconfiguration with more sophisticated features [29], [30], [31], [32], [33], [34], [35], [36].

All the antennas mentioned above are great options for the polarization reconfigurability. However, for the design advancement, their bias-isolation approach needs to be enhanced. Basically, the bias isolation can be achieved by means of two mechanisms: RF-DC coupling and decoupling. These two mechanisms are primarily related to the feed networks and radiating structures. The existing method utilizes either a DC block (capacitor) or a choke (inductor), which complicates the antenna structure with the redundant biasing lines. In some cases, a bias-T is used to function together with the antenna's feedlines for the bias coupling. However, without proper consideration of the decoupling mechanism, the antenna structure can still entail the extra lumped components for the bias isolation. This type of problem noticeably affects many reconfigurable single-element designs, making it challenging to advance as an array structure. This is due to the fact that as the array size expands, more DC blocks, choke components and biasing lines will be required. On the other hand, the reported array designs have made little progress in bias-isolation techniques. Instead, they are still relying on the supplementary passive components with the multilayer-based switching feed circuits for biasing. As a result, antenna fabrication becomes more intricate for assembling the circuit components and setting the precise alignment between the multiple substrates. Therefore, the bias-isolation method for electrical reconfiguration is fundamentally associated with the design improvement in planar integrated antenna technology.

In this paper, a new design for a planar integrated array is proposed to address the aforementioned issues. From the design perspective, the array architecture is constructed to be straightforward and effective for the targeted CP switching operation. Short-ended microstrip-line perturbations are used with the radiating components to reinforce the CP property with bias-decoupling characteristics. Meanwhile, magic-Ts are used to facilitate the array feed structure for the bias-coupling mechanism with high isolation features. By combining these two techniques in a single layer, the complete bias-isolation mechanism can eliminate any extraneous choke components and filters. Therefore, the proposed array demonstrates a simple and efficient design for the CP switching function, and its built-in bias-isolation circuit represents the state-of-the-art technology.

II. ANTENNA STRUCTURE AND DESIGN PROCEDURE

In this section, the design evolution process of the proposed array antenna will be discussed. Each design concept is aimed at implementing a single-layer-based simple biasing technique for the desired CP reconfigurable function. For this purpose, the array design is augmented to act as a built-in bias-isolation mechanism by interacting with the radiating components and feed structure.

Fig. 1 shows the structure of the proposed microstrip array antenna. The array consists of four CP reconfigurable elements and a magic-T integrated feed network. Two short-ended microstrip lines are integrated into each radiating element using diodes. In addition, the diodes are positioned to operate in both the positive and negative bias states for right-handed circular polarization (RHCP) and left-handed circular polarization (LHCP). For signal excitation, this array uses Port 1 and 2 for the RF and switching (DC) signals, respectively. For Port 1, a microstrip-slot branch is simply used, whereas, Port 2 effectively employs a microstrip-line branch. To simultaneously provide the RF and switching signals, magic-Ts are used for the signal coupling between these two ports with high isolation characteristics. The design

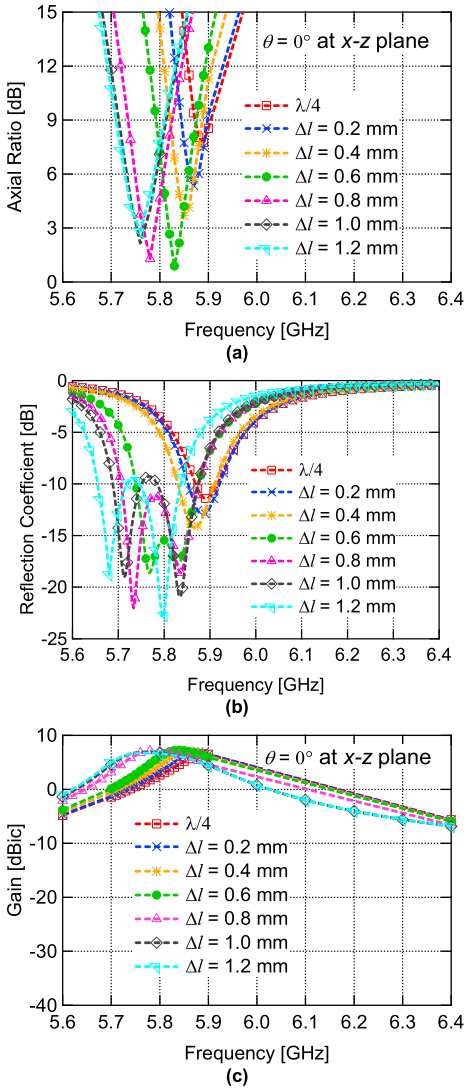

FIGURE 3. Parametric analysis of Δl. (a) axial ratio (b) reflection coefficient and (c) gain.

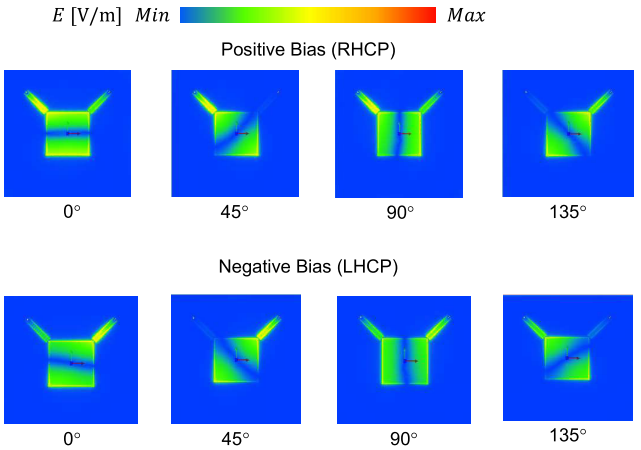

FIGURE 4. Simulated electric-field distribution for RHCP and LHCP excitations.

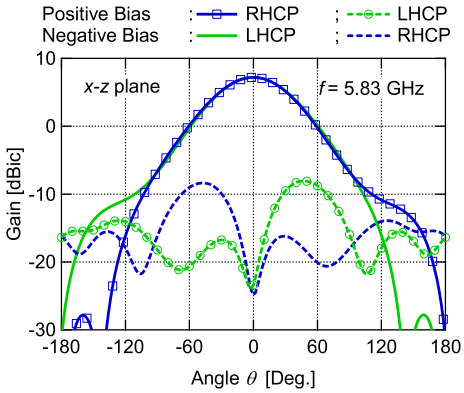

FIGURE 5. Radiation patterns of the CP reconfigurable element.

concept for the single reconfigurable element and magic-T feed network is also presented in the following sections.

A. RECONFIGURABLE CP PATCH ELEMENT

This section explains the design approach of a single-patch antenna. As discussed above, the short-ended microstrip lines are integrated with the radiating structures to assure the perturbation segment for bias-decoupling behavior. Therefore, a novel feature of the single element can be noticed in the RF-DC decoupling mechanism with CP switching operation.

Fig. 2 presents the schematic layout of a CP reconfigurable element. In this design, a square microstrip patch with a single-point feed is used as a radiating element. Two short-ended microstrip lines are also integrated with the upper corners of the radiating patch via switching diodes. Then, they are specifically designed to be $(\Delta l + \lambda/4)$ long. Here, Δl stands for the perturbation's length to provide CP, and a shorted $\lambda/4$ for an LC network to decouple the switching (DC) signal. Since these two functionalities are combined in a single microstrip line, it can operate as both a perturbation and a bias-decoupling network. Therefore, this single element can offer design flexibility for the CP switching characteristics without further any capacitors and inductors for the bias decoupling.

To confirm the proposed concept, a parametric analysis is performed with the aid of Keysight Technologies' EMPro. In the simulation, this reconfigurable element is designed for 5.8 GHz with the dimensions of $L_f = 16.1$ mm, $W_p = 2.4$ mm, and $L_g = 50$ mm. Here, the thickness and permittivity of the substrate are assumed to be 0.8 mm and 2.15, respectively. For the switching purpose, the diode's positive and negative switching states are modeled by a 3-Ω resistor and a 0.025-pF capacitor, respectively. A bias-T is also supposed to be used in the RF-DC coupling mechanism. In this analysis, two $\lambda/4$ microstrip lines are initially determined, and the parameter is studied to examine the effect of Δl. During analysis, all other parameters are fixed, and only Δl is tuned.

Fig. 3 demonstrates the effect of Δl for the axial ratio (AR), reflection coefficient and gain. In Fig. 3 (a), an AR

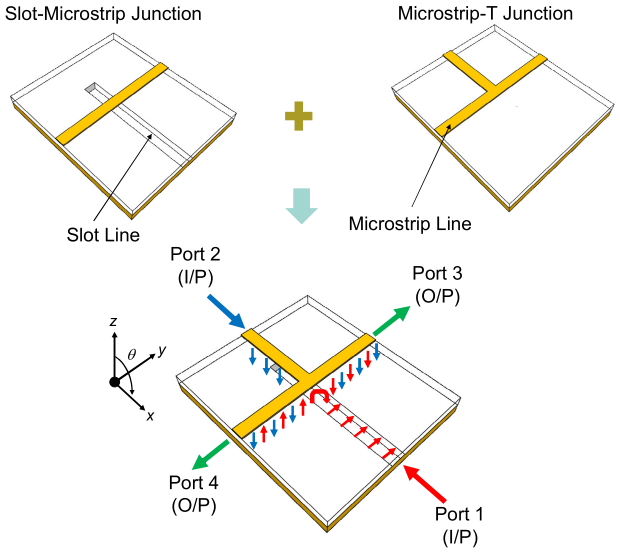

FIGURE 6. Structure of the single-section magic-T and its signal excitation mechanism.

frequency shift can be observed for every Δl change. In Fig. 3 (b), the reflection coefficient is progressively better than -10 dB when Δl is added to each $\lambda/4$ segment. In Fig.3 (c), the gain response is also shifting in accordance with the AR frequencies when adjusting Δl. Then, the best AR value is selected as the highest priority, and the other characteristics are examined based on that AR operating frequency. The overall analysis displays that an optimum AR value is attained at 5.83 GHz when Δl becomes 0.6 mm. At that perturbation length, AR frequency is also within the 10-dB impedance bandwidth and maintains a maximum gain as well.

Fig. 4 shows the simulated electric-field distribution of the CP reconfigurable element. As an operation, this element can be considered as either RHCP or LHCP excitation over the switching states. Then, the angular rotation of electric-field distribution is examined for the various time instants at 5.83 GHz. For a positive bias state, the electric null on the radiating element is orienting in anti-clockwise rotation. In this case, the patch element is operating for RHCP excitation. In a negative bias condition, the angular orientation of electric null is reversed, especially tracing in clockwise direction. In this case, the antenna again produces the CP with LHCP radiation.

Fig. 5 illustrates the simulated radiation patterns of the single reconfigurable element. After confirming the CP characteristics, the radiation patterns are examined in the *x*-*z* plane at 5.83 GHz. The simulation exhibits RHCP and LHCP gains of around 7 dBic for both the positive and negative switching states. The cross-polarization level is also better than 20 dB for each condition. In this way, the simulated results confirm that the short-ended microstrip-line perturbation is reliable for the CP switching with bias-decoupling feature.

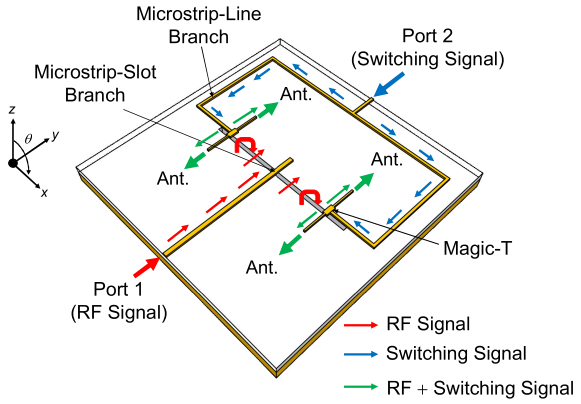

FIGURE 7. Structure of the proposed magic-T integrated feed network for 2 × 2 array configuration.

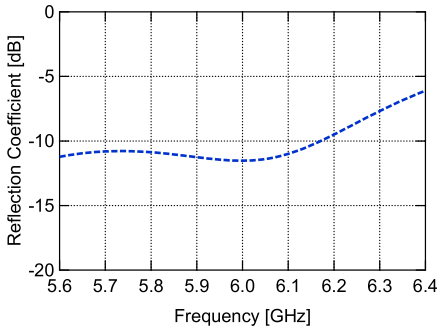

FIGURE 8. Simulated reflection coefficient of the magic-T integrated feed network.

B. MAGIC-T INTEGRATED FEED NETWORK

This section encompasses the array feed network for the RF-DC coupling mechanism. For the CP switching operation, each reconfigurable element requires the RF and switching (DC) signals concurrently. Therefore, in this array, magic-Ts are effectively utilized as a both-sided MIC technology to provide high isolation between the RF and switching signal ports.

Fig. 6 depicts a basic structure of the single-section magic-T. It includes four ports designed to intersect between the slot-microstrip and microstrip-T junctions. In this layout, Port 1 and 2 are considered for input signals, and Port 3 and 4 are for output terminals. Particularly, Port 1 (slot-microstrip junction) constitutes a series branch, whereas Port 2 (microstrip-T junction) forms a parallel branch. Therefore, when the signal is applied to Port 1, it will deliver to the output ports in terms of anti-phase propagation. For Port 2, the signal will be equally split between the two output terminals with an in-phase mode. On this basis, this magic-T circuit is applied for the RF-DC feeding method in this application.

Fig. 7 illustrates the structure of the magic-T integrated feed network. As mentioned above, the array's feed network is constructed with Port 1 and 2, which are respectively designated to the RF and switching signals. Here, Port 1 simply

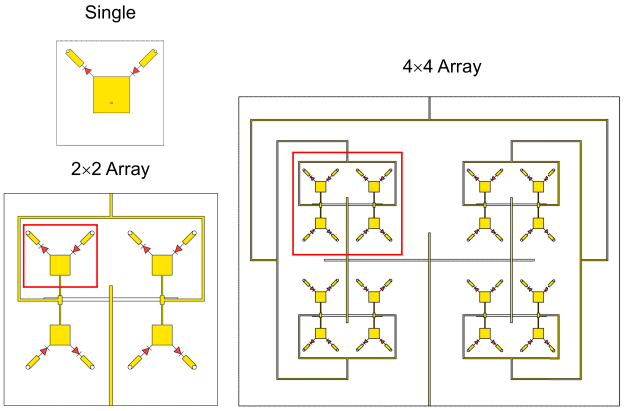

FIGURE 9. Design advantage of the proposed feed network with CP reconfigurable elements for large-scale array configuration.

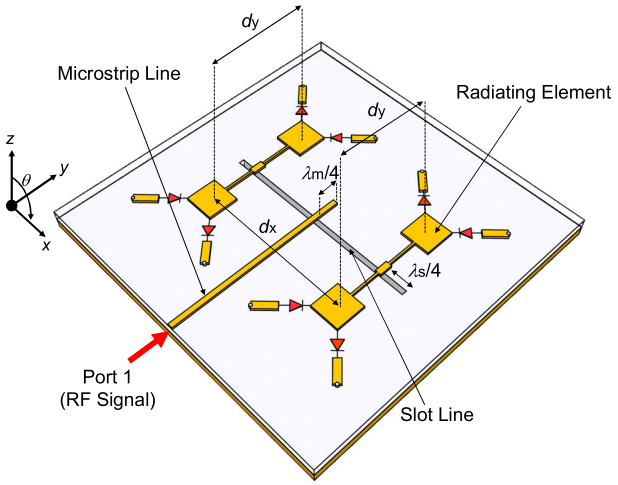

FIGURE 10. Structure of the 2 × 2 planar array for beam-forming optimization.

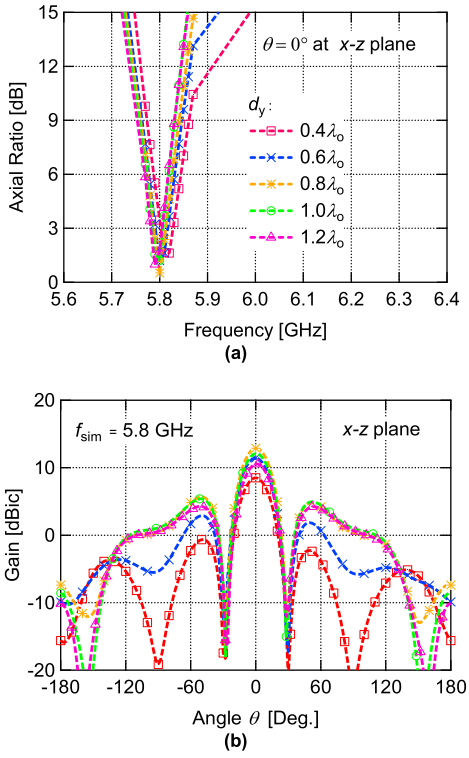

FIGURE 11. Parametric analysis of d_y. (a) axial ratio and (b) radiation pattern.

uses the microstrip line to excite the slot-microstrip junctions of the two magic-Ts. Therefore, for the RF signal, Port 1 is created to be an in-phase parallel microstrip-slot branch. On the other hand, Port 2 is further expanded by exclusively utilizing the microstrip lines for parallel T-junction. Hence, the switching signal can propagate in in-phase manner as discussed in the single-section layout. Consequently, Port 1 and 2 can highly be isolated due to the different propagation modes between the microstrip line and slot line. Furthermore, the other four ports are distributed for the antenna elements to realize the in-phase signal when the slot-microstrip junctions of the two magic-Ts are excited. For this reason, this array feed network can facilitate the broadside radiation pattern when the RF signal is applied to Port 1.

Fig. 8 demonstrates the simulated reflection coefficient of the magic-T based feed network shown in Fig. 7. In the simulation, a 200-Ω resistive load, which is equivalent to the antenna impedance at its radiating edge, is integrated into each output terminal. In this state, Port 1 shows better than 10-dB impedance bandwidth ranging from 5.6 to 6.15 GHz. However, Port 2 only concerns the switching (DC) signal, and therefore, its reflection is not essential to be considered in this array's feed network.

Fig. 9 shows the design advantage of the proposed array topology. An easy array expansion is achievable with no additional DC blocks, choke components and filters. This is due to the perfect design flexibility between the array feed network and radiating structures which can control the RF-DC coupling-decoupling mechanism for the bias isolation. In addition, as a further advancement, this array can be made possible for the differential-beam pattern in the *y-z* plane by applying the RF signal to Port 2. Therefore, in many array antenna topologies, magic-T inspired feed networks are extensively utilized for numerous purposes [37], [38], [39], [40], [41], [42], [43], [44], [45].

C. ARRAY DESIGN

This section emphasizes the array design using the radiating elements in Fig. 2. Unlike the proposed structure in Fig. 1, only Port 1 is utilized in this array, and the beam-forming behavior is investigated over the element spacing.

Fig. 10 demonstrates the structure of the 2 × 2 planar array antenna. In this configuration, the center-to-center distances between the radiating elements are expressed as d_x and d_y. The array's feed network has the microstrip-slot and slot-microstrip branches, and they are created using a single slot line with the several microstrip lines. For the microstrip-slot branch, an extended $\lambda_m/4$ segment of the

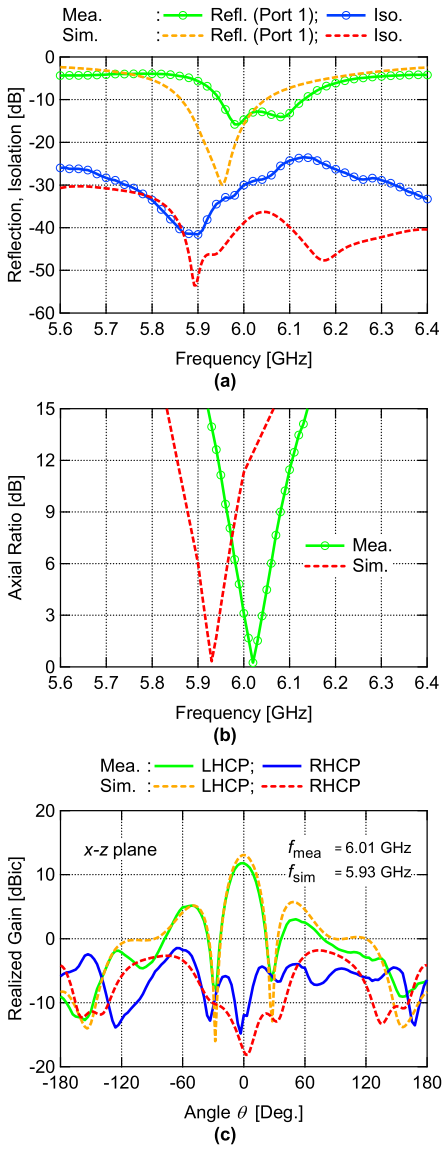

FIGURE 12. Simulated and measured results of the ideal array. (a) reflection and isolation, (b) axial ratio, and (c) radiation pattern.

center microstrip line represents a short circuit. Therefore, the signal can properly be excited to the slot line when the RF signal is applied to Port 1. For this branch, the impedance matching can be achieved by designing the slot line's impedance to be double that of the center microstrip line. On the other hand, the extended $\lambda_s/4$ sections of the slot line serve as the open circuits for the slot-microstrip branches. As a result, the RF signal can be routed to the radiating elements via the microstrip lines. The impedance matching for these branches can be made possible using the microstrip lines whose impedance is half that of the slot line. Then, the beam-forming behavior of the array is examined alongside with the CP characteristics. In this case, for the short brevity, the default value of d_x is initially set to $0.8\lambda_o$, and only d_y is altered for the parameter investigation.

Fig. 11 illustrates the impact of the element spacing (d_y) on the axial ratio and radiation pattern of the array. This study is also conducted using the Keysight Technologies' EMPro. As shown in Fig. 11 (a), the CP characteristics of the array is firstly explored at angle $\theta = 0°$ for the x-z plane. According to the simulated results, the array displays lower than 3-dB ARs at 5.8 GHz for every d_y spacing. Then, the array's radiation patterns are examined as a further step at 5.8 GHz for the x-z plane. In Fig. 11 (b), the array clearly shows the broadside patterns with the peak values at angle $\theta = 0°$ for each d_y change. Among the various element spacings, it is apparent that the broadside gain performance is at its best when d_y becomes $0.8\lambda_o$. Meanwhile, in this array, it can be noticed that the side lobe level also rises in accordance with the broadside gain. Based on these two evaluations, the array shows the satisfaction for the CP feature with optimum broadside gain pattern at $d_y = 0.8\lambda_o$. Consequently, it is observed that the element spacing in this array is the same for d_x and d_y.

III. MEASURED RESULTS

In this section, the performances of the proposed microstrip array antennas are experimentally discussed in comparison with the simulated data. Two prototype antennas are classified into the ideal and switching states depending on the type of radiating elements. Both arrays use a single-layer Polytetrafluoroethylene (PTFE) substrate, having permittivity (ε_r) of 2.15 and thickness (h) of 0.8 mm.

A. IDEAL-STATE CP ARRAY ANTENNA

Initially, an ideal array is developed to precisely analyze the antenna performance. Each radiating element is designed similarly to that in Fig. 2, except that no switching diodes are utilized. Instead, only the right corner is attached with the shorted perturbation, and the left corner is remained detached. In this manner, the upper two corners of the patch create the ideal short and open conditions. Then, using the array design in Fig. 1, these ideal radiating elements are positioned to each magic-T, and they are equally separated by $0.8\lambda_o$. Therefore, as an operation, this array can radiate the broadside LHCP pattern when the RF signal is routed to Port 1.

Fig. 12 demonstrates the simulated and measured performances of the ideal array. In Fig. 12 (a), the reflection coefficient provides 10-dB impedance bandwidth of 3.3% (5.85−6.05 GHz) for simulation. Meanwhile, measurement obtains around 2.9% (5.95−6.13 GHz). In addition, port isolation of better than 20 dB is realized within their respective 10-dB impedance bandwidths for both cases. In Fig. 12 (b), the simulation generates an AR at 5.92 GHz with a minimum value of 0.8 dB. Similarly, for measurement, it exhibits a minimum AR of around 0.8 dB at 6.01 GHz. In Fig. 12 (c), the radiation pattern is investigated in the x-z plane at their minimum AR frequencies. The broadside pattern is observed with the realized gain of around 12 dBic for simulation and 11 dBic for measurement. Also, both cases have better than 20-dB cross-polarization suppression. In this way, the ideal array is identified for CP characteristics based on the

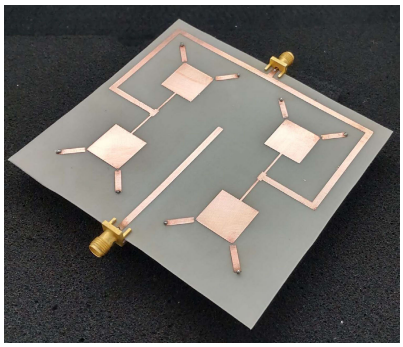

FIGURE 13. Photograph of a 5.8-GHz fabricated prototype (100 mm × 110 mm).

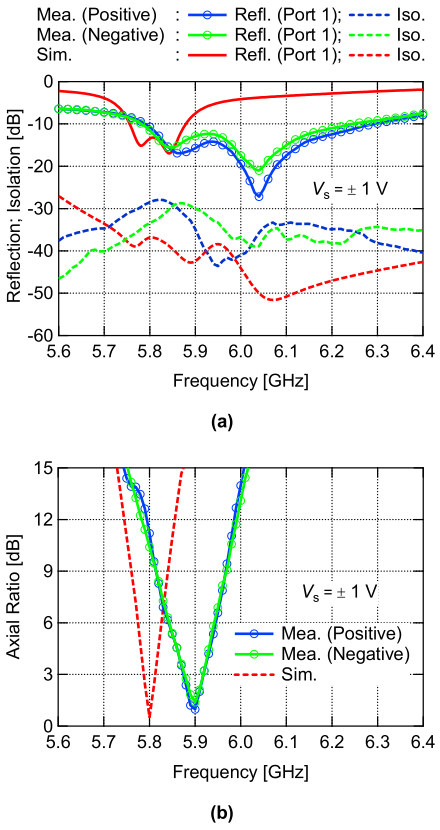

FIGURE 14. Simulated and measured results of the switching array. (a) reflection and isolation and (b) axial ratio.

simulated and measured results. Moreover, the feed network guarantees the high-isolation characteristics between Port 1 and 2. Therefore, the switching array is feasible to implement as a next step to investigate the CP reconfigurable operation with simple bias-isolation feature.

B. CP SWITCHABLE ARRAY ANTENNA

This section discusses our finalized design for CP switchable array antenna. The proposed array is designed for 5.8 GHz with the overall ground plane of 100 mm × 110 mm.

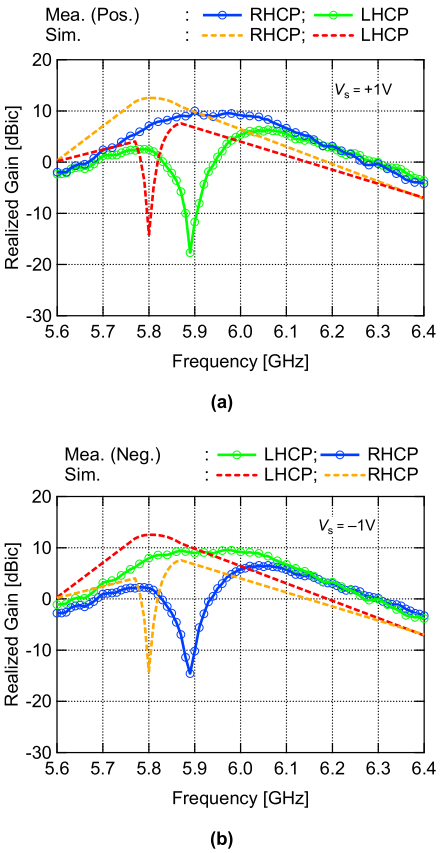

FIGURE 15. Simulated and measured realized gains of the switching array. (a) positive switching voltage and (b) negative switching voltage.

Then, the measurement is further conducted to check its performances.

Fig. 13 shows the 5.8-GHz fabricated prototype of the switching array. In this structure, a CP reconfigurable element discussed in Fig. 2 is established in array configuration. Diodes (DSM-8100-000, SKYWORK) are mounted between the radiating elements and short-ended microstrip lines for the switching property. In this case, the switching voltage (V_s) is set to ± 1V for the CP switching characteristics.

Fig. 14 illustrates the simulated and measured results of the reflection coefficient and axial ratio. As shown in Fig. 14 (a), the simulation produces 2.4% (5.75−5.89 GHz) 10-dB impedance bandwidth, whereas the measurement attains 7.6% (5.8−6.25 GHz). Also, both the simulation and measurement have better than 20-dB isolation within their respective 10-dB impedance bandwidths. In Fig. 14 (b), AR of lower than 3 dB is acquired for both simulation and measurement. The optimum AR frequencies can be distinguished at 5.8 GHz for simulation and 5.9 GHz for measurement. According to the measured results, 10-dB impedance bandwidths cover their corresponding 3-dB AR operating frequencies.

Fig. 15 presents the simulated and measured antenna's realized gains over frequency response. The peak realized

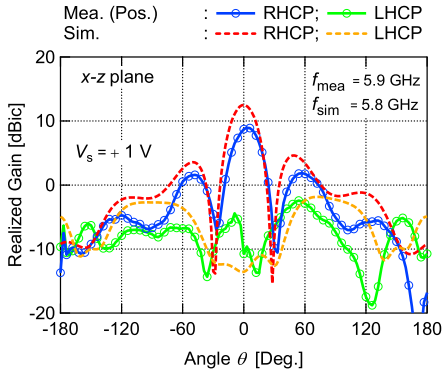

(a)

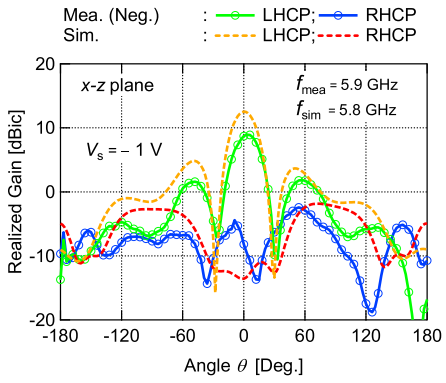

(b)

FIGURE 16. Simulated and measured radiation patterns of the switching array. (a) positive switching voltage and (b) negative switching voltage.

gains are observed at frequencies where minimum AR is obtained. Simulation produces an antenna realized gain of 12 dBic at 5.8 GHz, whereas, measurement provides around 10 dBic at 5.9 GHz. Both simulation and measurement exhibit the cross-polarization suppression of better than 20 dB at their corresponding minimum AR frequencies.

Fig. 16 depicts the simulated and measured radiation patterns over switching voltages. The radiation patterns are examined in the x-z plane based on the minimum AR frequencies. Both the positive and negative bias states achieve the broadside patterns at angle $\theta = 0°$ for RHCP and LHCP excitations. For the realized gains, the simulation generates 12 dBic, whereas the measurement has 9.9 dBic. Moreover, the cross-polarization suppression of around 20 dB is observed for both simulation and measurement. In this case, it can be noticed that some losses are found in the broadside realized gains of the switching array. Therefore, to investigate this issue, the realized gains for the ideal and switching array are further examined in terms of frequency response.

Fig. 17 demonstrates the simulated and measured realized gains over frequency response. The comparison is illustrated based on the LHCP realized gains for the ideal and switching array. In the simulation, the maximum realized gains are achieved at 5.93 and 5.8 GHz for the ideal and switching array, respectively. Similarly, in the case of measurement,

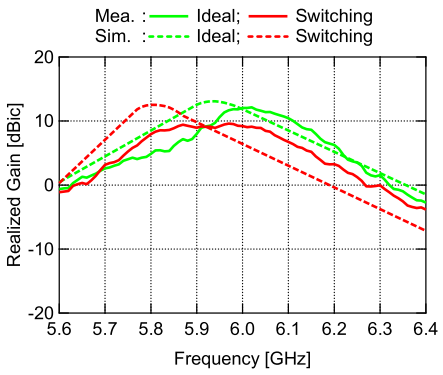

FIGURE 17. Simulated and measured realized gains over frequency response for the ideal and switching array.

both arrays still maintain the peak realized gain at 6 and 5.9 GHz. This implies that the realized gain response is better at their minimum AR frequencies for all cases. Additionally, it can be observed that the simulated realized gain responses for both arrays are nearly identical (around 12 dBic in each minimum AR frequency). Therefore, the loss between the ideal and switching array in simulation is almost negligible. However, according to the measured results, the switching array displays around 2 dB reduction in realized gain than that of the ideal array. As observed in Fig. 14 (a), these losses also contribute to an improvement in measured impedance bandwidth, which is about 3 times that of its simulated one.

Therefore, certain losses in the switching array can be assumed due to the power consumption of the diodes. It is reasonable to suppose that in the simulation, diodes are only considered for the switching purpose with the equivalent values of 3-Ω and 0.025-pF. These cases also imply that highly accurate diode models are required to improve the precision of simulated and measured results in the switching array. Moreover, the inconsistency between the EMPro's simulated design and the fabricated prototype shows some frequency shifts. Based on the minimum AR frequencies, the measured results in this array are approximately 100 MHz higher than the simulated results. Therefore, we simply understand that the array requires the optimization for frequency shift. But, in this instance, it has to be clarified that the prototype antennas are fabricated for the concept confirmation. If we can fabricate professionally with a high-precision machine and measurement setups, these error percentages can be minimized. However, despite some mismatches, the proposed array is still promising for CP reconfigurable functionality in terms of achieving performances in measurement.

Table 1 describes the comparison among electrically reconfigurable polarization antennas. The antenna design configurations are analyzed in relation to other necessary specifications across a ten-year technology trend. It is observed that the single-layer designs mentioned in [12], [14], and [17] have wider impedance and AR bandwidths due to high dielectric constants of their substrates. On the other hand, the multi-layer-based structures meticulously consider

TABLE 1. Comparison among electrically-controlled polarization reconfigurable antennas.

Ref.	Antenna Overall Size (λ_o)	Substrate Layer	Substrate Dielectric Constant	Antenna Type	Polarization Switching States	Auxiliary Bias-Isolation Components	Impedance BW (%)	AR BW (%)	Peak Realized Gain (LP: dBi, CP: dBic)
[10]	0.4×0.4×0.01	Multi	4.4	Ring slot	LP Dual-CP	Required	LP: 18.9 CP: 23.0	LHCP: 6.5 RHCP: 6.8	LP: 2.82 CP: 3.24
[12]	0.56×0.56×0.01	Single	4.2	Microstrip patch	Dual-CP	Required	5.62	2	3.17
[13]	0.56×0.56×0.13 (Reflector height: 15 mm)	Multi	4.2	Microstrip patch	LP Dual-CP	Required	LP: 3.10 CP: 11.3	2.27	7.26
[14]	0.28×0.54×0.01	Single	3.5	Monopole	LP Dual-CP	Required	LP: 70 CP: 22	LHCP: 4.4 RHCP: 4.5	LP: 0.5 CP: 1.2
[15]	0.4×0.08 (Reflector height: 9.43mm)	Multi	2.33	Microstrip patch	Dual-CP	Required	LP: 20 CP: 20	4	7
[17]	0.48×0.48×0.05	Single	3.3	Microstrip patch	Dual-CP	Required	7	4.085	4.9
[23]	0.8×0.26 (Reflector height: 50 mm)	Multi	2.65	Folded microstrip patch	Dual-CP	Required	80	23.5	4.8
[24]	1.2×1.2×0.22	Multi	3.5	Printed loop	Dual-CP	Required	32	LHCP: 14.9 RHCP: 12.7	8
[26]	0.59×0.59×0.24 (Reflector height: 55 mm)	Multi	2.2	Crossed dipole	Dual-CP	Required	53.3	58.9	9.1
[28]	0.58×0.58×0.24	Multi	3.38	Slot aperture coupled patch	LP to CP	Required	35.3	12.6	LP: 8.9 CP: 9.0
[30]	1×1×0.07	Multi	3.48	Planar array	Dual-CP	Required	14.9	LHCP: 3.6 RHCP: 4.3	9.6
[33]	0.05 (Overall height: 20 mm)	Multi	4.4	Crossed bow-tie	Dual-CP	Required	Overlapped BW: 21.7		13
[34]	1.3×1.3×0.01	Single	2.2	Planar array	45° LP Dual-CP	Required	< 6	< 1	10
[36]	1.41×1.41×0.035	Multi	2.2	Trapezoidal-shaped dipole	Multi-LPs	Required	5LPs: 20.6 7LPs: 17.6 9LPs: 15.9	NA	5LPs: 8.3 7LPs: 8.5 9LPs: 8.4
This work	1.9×2.1×0.01	Single	2.15	Planar array	Dual-CP	Not required	7.6	< 1	9.9

the heights of the antennas, which are primarily supported by the reflector. Therefore, the performances of such antennas are proven to be superior than those of the single-layer-based designs. In our proposed design, the array utilizes the single-layer-based design technology, and its characteristics perform similarly to the design indicated in [34]. Additionally, its measured peak realized gain performance is comparable to other multilayer-based designs. For all the cases, in contrast to the proposed design, all other reported configurations demand supplementary bias-isolation components for polarization reconfiguration. Therefore, this proposed design is the first experimentally-validated planar array antenna with the CP switching characteristics, requiring no auxiliary DC-blocking capacitors, choke inductors and bias-T for bias-isolation operation.

IV. CONCLUSION

This paper demonstrates a simple and efficient design of the polarization reconfigurable antenna. Planar integrated array technology is utilized to achieve the CP reconfiguration with simple biasing layout. Short-ended microstrip-line perturbations guarantee the CP and bias-decoupling properties

for each radiating element. Meanwhile, magic-Ts offer the RF-DC coupling with high port-isolation characteristics for the array feed network. As a result, the entire biasing mechanism can functionally be regulated in a single-layer substrate with no additional lumped components and filters. The excellent combination of these two techniques shows a novel perspective for the antenna design technology with built-in bias-isolation mechanism. This concept can be extended to future high-performance inspired electrically-controlled antenna designs. The agreement between the simulated and measured results also serves as the reliability of the proposed array. Moreover, the array shows its best performance with the peak realized gains of 9.9 dBic for both polarizations at minimum AR frequencies. Therefore, the proposed array is suitable for the applications, where precise frequency targeting is required, such as point-to-point communication systems.

ACKNOWLEDGMENT

The authors would like to thank Dr. Takayuki Tanaka and Dr. Maodudul Hasan, Saga University for their fruitful suggestions.

REFERENCES

[1] X. Yan, L. Li, H. C. Zhang, and J. Y. Han, "Broadband polarization-reconfigurable liquid dielectric resonator antenna controlled by gravity," *IEEE Antennas Wireless Propag. Lett.*, vol. 21, no. 10, pp. 2105–2109, Oct. 2022.

[2] J.-S. Row and M.-J. Hou, "Design of polarization diversity patch antenna based on a compact reconfigurable feeding network," *IEEE Trans. Antennas Propag.*, vol. 62, no. 10, pp. 5349–5352, Oct. 2014.

[3] A. Soltan, A. A. Abdulmajid, and S. K. Khamas, "Optically controlled circularly polarized-reconfigurable millimeter-wave rectangular dielectric resonator antenna using photoconductive switches," in *Proc. 16th Eur. Conf. Antennas Propag. (EuCAP)*, Madrid, Spain, Mar. 2022, pp. 1–5.

[4] Z. Hu, S. Wang, Z. Shen, and W. Wu, "Broadband polarization-reconfigurable water spiral antenna of low profile," *IEEE Antennas Wireless Propag. Lett.*, vol. 16, pp. 1377–1380, 2017.

[5] J. Tak and J. Choi, "Reconfigurable single port triangular patch antenna with polarization diversity," in *Proc. Int. Workshop Antenna Technol. (iWAT)*, Seoul, South Korea, Mar. 2015, pp. 130–133.

[6] M. A. Rahman, E. Nishiyama, Md. A. Hossain, Q. Delwar Hossain, and I. Toyoda, "A microstrip antenna with circular polarization switching capability for X-band applications," in *Proc. Int. Symp. Antennas Propag. (ISAP)*, Okinawa, Japan, Oct. 2016, pp. 820–821.

[7] M. A. Rahman, E. Nishiyama, and I. Toyoda, "A frequency diversity reconfigurable antenna with circular polarization switching capability," in *Proc. IEEE Int. Symp. Antennas Propag. USNC/URSI Nat. Radio Sci. Meeting*, San Diego, CA, USA, Jul. 2017, pp. 1367–1368.

[8] H. W. Htun, E. Nishiyama, and I. Toyoda, "A reconfigurable circularly polarized microstrip antenna with short-ended microstrip line perturbations," in *Proc. Int. Symp. Antennas Propag. (ISAP)*, Osaka, Japan, Jan. 2021, pp. 723–724.

[9] Z.-X. Yang, H.-C. Yang, J.-S. Hong, and Y. Li, "Bandwidth enhancement of a polarization-reconfigurable patch antenna with stair-slots on the ground," *IEEE Antennas Wireless Propag. Lett.*, vol. 13, pp. 579–582, 2014.

[10] C.-Y.-D. Sim, Y.-J. Liao, and H.-L. Lin, "Polarization reconfigurable eccentric annular ring slot antenna design," *IEEE Trans. Antennas Propag.*, vol. 63, no. 9, pp. 4152–4155, Sep. 2015.

[11] P. L. Huang, K. Chun Huang, H. N. Chu, and T.-G. Ma, "A reconfigurable T-shaped slot antenna using characteristic mode analysis," in *Proc. Int. Symp. Antennas Propag. (ISAP)*, Jan. 2021, pp. 713–714.

[12] S. W. Lee and Y. J. Sung, "Reconfigurable rhombus-shaped patch antenna with Y-shaped feed for polarization diversity," *IEEE Antennas Wireless Propag. Lett.*, vol. 14, pp. 163–166, 2015.

[13] S. W. Lee and Y. J. Sung, "Simple polarization-reconfigurable antenna with T-shaped feed," *IEEE Antennas Wireless Propag. Lett.*, vol. 15, pp. 114–117, 2016.

[14] A. Panahi, X. L. Bao, K. Yang, O. O'Conchubhair, and M. J. Ammann, "A simple polarization reconfigurable printed monopole antenna," *IEEE Trans. Antennas Propag.*, vol. 63, no. 11, pp. 5129–5134, Nov. 2015.

[15] K. M. Mak, H. W. Lai, K. M. Luk, and K. L. Ho, "Polarization reconfigurable circular patch antenna with a C-shaped," *IEEE Trans. Antennas Propag.*, vol. 65, no. 3, pp. 1388–1392, Mar. 2017.

[16] M. Patriotis, F. N. Ayoub, C. G. Christodoulou, and S. K. Jayaweera, "Polarization reconfigurable circular patch," in *Proc. IEEE Int. Symp. Antennas Propag. USNC-URSI Radio Sci. Meeting (APS/URSI)*, Singapore, Dec. 2021, pp. 753–754.

[17] C.-E. Guan, T. Fujimoto, and S. Iwasaki, "Polarization-agile circular polarized antenna based on proximity feeding technique," *IEEE Antennas Wireless Propag. Lett.*, vol. 20, no. 9, pp. 1636–1640, Sep. 2021.

[18] H. W. Htun, M. Hasan, E. Nishiyama, and I. Toyoda, "A reconfigurable circularly-polarized ring-slot antenna employing microstrip-line switchable feed network," in *Proc. Int. Symp. Antennas Propag. (ISAP)*, Oct. 2022, pp. 47–48.

[19] E. Nishiyama, A. Matsuo, and I. Toyoda, "Double balanced multiplier integrated circular polarization switchable microstrip antenna," in *Proc. IEEE Int. Symp. Antennas Propag. USNC/URSI Nat. Radio Sci. Meeting*, Vancouver, BC, Canada, Jul. 2015, pp. 2239–2240.

[20] E. Nishiyama, T. Ino, and I. Toyoda, "Experimental study of double-balanced-multiplier integrated circularly polarized microstrip antenna with nonlinear characteristics," in *Proc. Int. Symp. Antennas Propag. (ISAP)*, Oct. 2017, pp. 1–2.

[21] E. Nishiyama, H. Matsui, and I. Toyoda, "Circular polarization agile microstrip antenna with double balanced multiplier on ring slot," in *Proc. IEEE Int. Symp. Antennas Propag. USNC/URSI Nat. Radio Sci. Meeting*, San Diego, CA, USA, Jul. 2017, pp. 1145–1146.

[22] T. Kayashima, E. Nishiyama, and I. Toyoda, "Novel simulation approach to microstrip antenna integrated with nonlinear circuit," in *Proc. Int. Symp. Antennas Propag. (ISAP)*, Osaka, Japan, Jan. 2021, pp. 187–188.

[23] W. Lin and H. Wong, "Wideband circular polarization reconfigurable antenna," *IEEE Trans. Antennas Propag.*, vol. 63, no. 12, pp. 5938–5944, Dec. 2015.

[24] L. Zhang, S. Gao, Q. Luo, P. R. Young, and Q. Li, "Wideband loop antenna with electronically switchable circular polarization," *IEEE Antennas Wireless Propag. Lett.*, vol. 16, pp. 242–245, 2017.

[25] H. H. Tran and H. C. Park, "Wideband reconfigurable antenna with simple biasing circuit and tri-polarization diversity," *IEEE Antennas Wireless Propag. Lett.*, vol. 18, no. 10, pp. 2001–2005, Oct. 2019.

[26] H. H. Tran, N. Nguyen-Trong, T. K. Nguyen, and A. M. Abbosh, "Bandwidth enhancement utilizing bias circuit as parasitic elements in a reconfigurable circularly polarized antenna," *IEEE Antennas Wireless Propag. Lett.*, vol. 17, no. 8, pp. 1533–1537, Aug. 2018.

[27] Q. Chen, J.-Y. Li, G. Yang, B. Cao, and Z. Zhang, "A polarization-reconfigurable high-gain microstrip antenna," *IEEE Trans. Antennas Propag.*, vol. 67, no. 5, pp. 3461–3466, May 2019.

[28] Y. Zhang, Y. Zhang, K. Huang, S.-J. Liu, X. Y. Zhang, and Q. H. Liu, "A reconfigurable patch antenna with linear and circular polarizations based on double-ring-slot feeding structure," *IEEE Trans. Antennas Propag.*, vol. 70, no. 12, pp. 11389–11400, Dec. 2022.

[29] J.-S. Row, C.-Y.-D. Sim, and K.-W. Lin, "Broadband printed ring-slot array with circular polarization," *Elect. Lett.*, vol. 41, no. 3, pp. 110–112, Feb. 2005.

[30] W. Li, S. Gao, Y. Cai, Q. Luo, M. Sobhy, G. Wei, J. Xu, J. Li, C. Wu, and Z. Cheng, "Polarization-reconfigurable circularly polarized planar antenna using switchable polarizer," *IEEE Trans. Antennas Propag.*, vol. 65, no. 9, pp. 4470–4477, Sep. 2017.

[31] J. M. Kovitz, H. Rajagopalan, and Y. Rahmat-Samii, "Design and implementation of broadband MEMS RHCP/LHCP reconfigurable arrays using rotated E-shaped patch elements," *IEEE Trans. Antennas Propag.*, vol. 63, no. 6, pp. 2497–2507, Jun. 2015.

[32] M. Shirazi, T. Li, J. Huang, and X. Gong, "A reconfigurable dual-polarization slot-ring antenna element with wide bandwidth for array applications," *IEEE Trans. Antennas Propag.*, vol. 66, no. 11, pp. 5943–5954, Nov. 2018.

[33] W. Lin, S.-L. Chen, R. W. Ziolkowski, and Y. J. Guo, "Reconfigurable, wideband, low-profile, circularly polarized antenna and array enabled by an artificial magnetic conductor ground," *IEEE Trans. Antennas Propag.*, vol. 66, no. 3, pp. 1564–1569, Mar. 2018.
[34] M. Ikram, N. Nguyen-Trong, and A. Abbosh, "A simple single-layered continuous frequency and polarization-reconfigurable patch antenna array," *IEEE Trans. Antennas Propag.*, vol. 68, no. 6, pp. 4991–4996, Jun. 2020.
[35] Y. Cheng and Y. Dong, "A high-efficiency electrically reconfigurable circular polarizer and its array application," *IEEE Antennas Wireless Propag. Lett.*, vol. 20, no. 12, pp. 2314–2318, Dec. 2021.
[36] D. Chen, Y. Liu, S.-L. Chen, P.-Y. Qin, and Y. J. Guo, "A wideband high-gain multilinear polarization reconfigurable antenna," *IEEE Trans. Antennas Propag.*, vol. 69, no. 7, pp. 4136–4141, Jul. 2021.
[37] M. Aikawa and H. Ogawa, "A new MIC magic-T using coupled slot lines," *IEEE Trans. Microw. Theory Techn.*, vol. MTT-28, no. 6, pp. 523–528, Jun. 1980.
[38] M. Aikawa and H. Ogawa, "Double-sided MICs and their applications," *IEEE Trans. Microw. Theory Techn.*, vol. 37, no. 2, pp. 406–413, Feb. 1989.
[39] J. P. Kim and W. S. Park, "Novel configurations of planar multilayer magic-T using microstrip-slotline transitions," *IEEE Trans. Microw. Theory Techn.*, vol. 50, no. 7, pp. 1683–1688, Jul. 2002.
[40] S. Gruszczynski and K. Wincza, "Broadband high-performance coupled-line magic-T network for direction finding systems," in *Proc. IEEE Antennas Propag. Soc. Int. Symp.*, Honolulu, HI, USA, Jun. 2007, pp. 2085–2088.
[41] K. Yen, E. J. Wollack, J. Papapolymerou, and J. Laskar, "A broadband planar magic-T using microstrip–slotline transitions," *IEEE Trans. Microw. Theory Techn.*, vol. 56, no. 1, pp. 172–177, Jan. 2008.
[42] M. A. Hossain, E. Nishiyama, M. Aikawa, and I. Toyoda, "Multi-band orthogonal linear polarization discrimination planar array antenna," *Prog. Electromagn. Res. C*, vol. 34, pp. 53–67, 2013.
[43] Md. A. Hossain, P. Chowdhury, Q. D. Hossain, E. Nishiyama, and I. Toyoda, "Design of a circular polarization switchable microstrip array antenna using magic-T bias circuit," in *Proc. Int. Conf. Electr. Inf. Commun. Technol. (EICT)*, Feb. 2014, pp. 1–4.
[44] N. Morita, T. Tanaka, and I. Toyoda, "A variable power divider employing magic-T and variable phase shifter," *IEEE Microw. Wireless Compon. Lett.*, vol. 31, no. 6, pp. 565–568, Jun. 2021.
[45] Y. Umeda, E. Nishiyama, and I. Toyoda, "A beam-forming antenna integrating magic-T based matrix feed network," in *Proc. Int. Symp. Antennas Propag. (ISAP)*, Oct. 2022, pp. 433–434.

HTET WAI HTUN (Graduate Student Member, IEEE) was born in Kyauktan, Yangon Region, Myanmar, in 1996. He received the B.E. degree from Technological University, Thanlyin, Myanmar, in 2019, and the M.E. degree from the Department of Electrical and Electronic Engineering, Saga University, Japan, in 2021, where he is currently pursuing the Ph.D. degree with the Communication Engineering Laboratory. His research interests include planar antennas and advanced reconfigurable antennas and its array designs. He was a recipient of the "2019 Excellent Presentation Award" presented by the IEEE Fukuoka Section.

EISUKE NISHIYAMA (Member, IEEE) was born in Saga, Japan. He received the degree from the Department of Electrical and Electronic Engineering, Saga University, in 1987, the M.S. degree, in 1989, and the Dr.Eng. degree. He was a Research Associate, from 1997 to 2007, and an Assistant Professor, from 2007 to 2017. He was a member of the technical staff with the Department of Electrical and Electronic Engineering, Saga University. He was a Visiting Scholar with UCLA, from 2007 to 2008. He has been an Associate Professor, since 2017. His research interests include planar antennas, especially integrated functional antennas. He was the Chair of the IEEE AP-S Fukuoka Chapter, from 2013 to 2014.

ICHIHIKO TOYODA (Member, IEEE) received the B.E., M.E., and Dr.Eng. degrees in communication engineering from Osaka University, Osaka, Japan, in 1985, 1987, and 1990, respectively. From 1990 to 2011, he was engaged in research and development of the three-dimensional (3-D) and uniplanar MMICs, ultra-high-speed digital ICs, millimeter-wave high-speed wireless access systems and their applications with NTT Laboratories and NTT Electronics Corporation. He was also active in developing IEEE 802.11, 802.15, and other national standards. He is currently a Professor and the Dean of the Faculty of Science and Engineering, Saga University, Japan. He has published six book chapters. His current research interests include microwave circuits, antennas and their integration technologies, including wireless power transfer. He is a Senior Member of IEICE and IEEJ and a member of the European Microwave Association (EuMA). He received the 1993 Young Researcher's Award presented by the IEICE, Japan; the Japan Microwave Prize presented from the APMC1994; the 18th Telecom System Technology Award from the Telecommunications Advancement Foundation; the 2004 Electronics Society Award from the IEICE; the First Prize for Propagation and Antenna Measurements from the EuCAP2010; the 2010 and 2016 Best Paper Awards from the IEICE; the 2020 Best Paper Award from Institute of Electrical Engineers of Japan (IEEJ), Japan, and many conference and NTT research and development awards. He was recognized as an Excellent Educator by Saga University, in 2017. He was a Councilor of the Tokyo Section and the Kyushu Section, IEICE and a GA member of EuMA. He was the Chair of the IEEE AP-S Fukuoka Chapter. He served Technical Committee on Electron Devices of IEEJ, as a Secretary, the Vice-Chair, and the Chair. He also served on many other technical committees of IEICE and IEEJ. He was the Guest Editor of the 1998 Special Issue on "3D-Components and Active Circuits" of the *International Journal of RF and Microwave Computer-Aided Engineering* and the Guest Editor-in-Chief of the 2016 Special Issue on "Microwave Researches in Universities" of the Institute of Electronics, Information and Communication Engineers and *IEICE Transactions on Electronics*.